Stress and strain in the anterior band of the inferior glenohumeral ligament during a simulated clinical examination

Richard E. Debski, PhD,[ab] Jeffrey A. Weiss, PhD,[c] William J. Newman,[c] Susan M. Moore,[b] and Patrick J. McMahon, MD,[a] Pittsburgh, PA, and Salt Lake City, UT

The objective of this research was to predict, with a finite-element model, the stress and strain fields in the anterior band of the inferior glenohumeral ligament (AB-IGHL) during application of an anterior load with the humerus abducted. The stress and strain in the AB-IGHL were determined during a simulated simple translation test of a single intact shoulder. A 6–degree-of-freedom magnetic tracking system was used to measure the kinematics of the humerus with respect to the scapula. A clinician applied an anterior load to the humerus until a manual maximum was achieved at 60° of glenohumeral abduction and 0° of flexion/extension and external rotation. For the computational analysis, the experimentally measured joint kinematics were used to prescribe the motion of the humerus with respect to the scapula, whereas the material properties of the AB-IGHL were based on published experimental data. The geometry of the AB-IGHL, humerus, and scapula was acquired by use of a volumetric computed tomography scan, which was used to define the reference configuration of the AB-IGHL. Strains reached 12% along the inferior edge and 15% near the scapular insertion site at the position of maximum anterior translation. During this motion, the AB-IGHL wrapped around the humerus and transferred load to the bone via contact. Predicted values for von Mises stress in the ligament reached 4.3 MPa at the point of contact with the humeral head and 6.4 MPa near the scapular insertion site. A comparison of these results to the literature suggests that the computational approach provided reasonable predictions of fiber strain in the AB-IGHL when specimen-specific geometry and kinematics with average material properties were used. The complex stress and strain distribution throughout the AB-IGHL suggests that the continuous nature of the glenohumeral capsule should be considered in biomechanical analyses. In the future, this combined experimental and computational approach will be used for subject-specific studies of capsular function and could provide quantitative data to help surgeons improve methods for the diagnosis and treatment of glenohumeral instability. (J Shoulder Elbow Surg 2005;14: 24S-31S.)

Glenohumeral stability is maintained through a complex combination of bony contact and soft-tissue restraints that include the joint capsule and muscles. However, the role of the glenohumeral capsule in joint stability has continued to be a source of controversy because of its complex geometry and the large range of motion of the shoulder. Several studies have emphasized the band-like appearance of the various thickenings throughout the glenohumeral capsule, referred to as the glenohumeral ligaments. The gross and histologic appearance of the inferior region of the glenohumeral capsule (inferior glenohumeral ligament [IGHL]) has been investigated.[23] In the past, biomechanical analyses have most commonly used selective sectioning experiments to determine the role of this region in providing joint stability.[6,8,35] These studies have suggested that the IGHL is the most important passive stabilizer in the anterior direction when the shoulder is abducted and externally rotated.

To gain further insight to the function of this region of the glenohumeral capsule, investigators have examined the elongation of the capsule throughout joint motion by quantifying either uniaxial strain in localized regions or length changes of the IGHL by use of the origin-to-insertion distance.[2,7,19,24,32,35,36] In ad-

dition, the forces in this region of the glenohumeral capsule have been evaluated qualitatively by palpation during cadaveric dissections[4,21,22,25] or estimated indirectly by use of mercury strain gauges mounted on the outside of the joint capsule.[32] However, uniaxial analyses cannot measure or predict the load that is transferred to the humerus as the glenohumeral capsule wraps around the humeral head. Furthermore, a recent biomechanical study has demonstrated that the strain in the anteroinferior region of the glenohumeral capsule is not uniaxial.[14] Therefore, experimental and computational models should account for the 3-dimensional geometry of the capsule. In addition, understanding the stress and strain distribution in the capsule could help improve surgical procedures for repair of damaged tissue and guide surgeons in performing an examination with patients under anesthesia.

The objective of this study was to predict, with a finite-element analysis, the stress and strain field in the anterior band of the inferior glenohumeral ligament (AB-IGHL) during application of an anterior load with the humerus abducted. The overall hypothesis was that a complex stress and strain distribution exists in the AB-IGHL as a result of its continuous nature and its wrapping around the humeral head.

MATERIALS AND METHODS

Experimental measurement of shoulder kinematics

A fresh-frozen cadaveric shoulder specimen (female, aged 64 years) was stored within 2 plastic bags and maintained at −20°C until dissection. Before dissection, the specimen was thawed overnight at room temperature. The specimen was dissected free of all soft tissue except the rotator cuff tendons, glenohumeral joint capsule, and coracoacromial ligament. At this time, no signs of arthritis or previous soft-tissue injury were found. The capsule was vented to atmospheric pressure at the rotator interval during the dissection process. The scapula and humerus were fixed in molds of epoxy putty, such that the medial margin of the scapula was vertical, the plane of the scapula was parallel to the surface of the block, and the long axis of the humerus was centered and parallel to the central axis of the cylinder. Nylon tethers were sutured to the tendons of the supraspinatus, subscapularis, and infraspinatus/teres minor, allowing loads to be applied to each rotator cuff tendon via a pulley system.[16] Plexiglas registration blocks were affixed to the scapula and humerus. The edges of these blocks were used to form local coordinate systems, and the block geometry allowed coregistration of the kinematic and computed tomography (CT) data sets.[5]

The scapula was mounted rigidly to a Plexiglas fixture. A sensor for a 6–degree-of-freedom magnetic
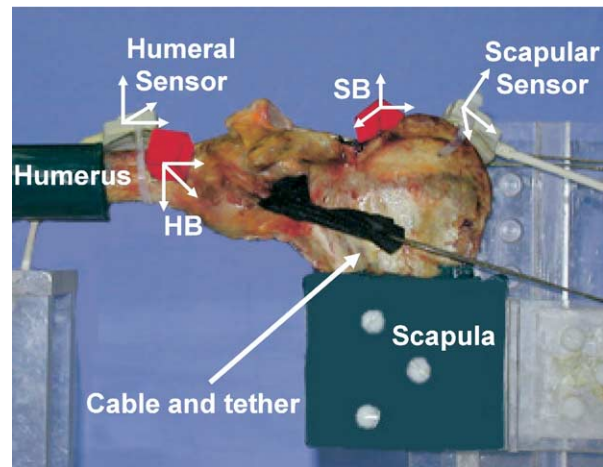

Figure 1 Experimental setup with the cadaveric shoulder fixed to the testing jig. The coordinate systems of the humeral sensor, scapular sensor, humeral registration block (*HB*), and scapular registration block (*SB*) are shown.

tracking system[28,34] (Flock of Birds; Ascension Technologies Corporation, Burlington, VT) was attached to the medial margin of the scapula. A second sensor was fixed to the humerus, distal to the humeral head (Figure 1). A pulley system and weights were used to apply 13.4 N to each rotator cuff tendon to simulate in vivo rotator cuff muscle tension during a clinical examination.[3,11,36]

The humerus was then fixed at 90° of glenohumeral abduction, 0° of flexion/extension (in line with scapular plane), and 0° of internal/external rotation. The longitudinal axis of the bicipital groove and anterior edge of the acromion were used to determine the reference position for internal/external rotation of the humerus as previously described.[18,33] The coordinate systems of the humerus and scapula were then defined by use of anatomic landmarks digitized with a third sensor attached to a stylus. The most anterior point of the lesser tuberosity and the most posterior point of the humeral head were digitized. The point midway between the anterior and posterior points was established as the origin for both the scapular and humeral coordinate systems. The longitudinal axis of the humerus was determined by digitizing along the epoxy putty cylinder of the humerus, and the scapular plane was established by digitizing along the anterior surface of the epoxy putty block of the scapula. With the use of these anatomic landmarks, orthonormal coordinate systems were created.

For a right shoulder, the x-, y-, and z-axes of the humerus and scapula were oriented positively in the anterior, superior, and lateral direction, respectively. The orientation of the humerus with respect to the scapula was determined by use of a rotation sequence about the axes of the humerus. The first rota-

tion was about the x-axis of the humerus and corresponded to glenohumeral adduction/abduction. The second rotation was about the y-axis and defined flexion/extension. The final rotation defined internal/external rotation and was about the z-axis of the humerus. Throughout the range of motion of the glenohumeral joint, the sensors were a maximum of approximately 300 mm apart. Accuracy of the magnetic sensors was previously determined to be less than 0.3% of the distance between the sensors and less than 1.0°.[41]

Once the anatomic coordinate systems were determined, the local coordinate systems for coregistration of the kinematic and CT data sets were established at the registration blocks. With the glenohumeral joint in the reference position, the sensor used to digitize the anatomic landmarks was used to digitize 3 faces of each registration block. From these data, local coordinate systems were created for each registration block[5] and the constant relationship between the anatomic coordinate system and the registration block of each bone was determined. Therefore, the motion of the humeral registration block with respect to the scapular registration block could be determined from the motion of the anatomic coordinate systems of the humerus and scapula.

For the following experimental protocol, the clinician was provided information regarding the angular position of the humerus. The humerus was rotated to its starting position of 60° of glenohumeral abduction (corresponding approximately to 90° of shoulder abduction in the body[10,26]), 0° of flexion/extension, and 0° of internal/external rotation. A simple translation test in the anterior direction[29] was defined as a clinical test in which the humerus was oriented at 60° of glenohumeral abduction and 0° of flexion/extension, while the clinician applied an anterior load to the humerus until a manual maximum was achieved at 0° of external rotation. This process was sequentially repeated 3 times. To minimize viscoelastic affects, the first 3 sequences were used to precondition the tissue.

CT scan, geometry reconstruction, and mesh generation

Insertion site locations of the AB-IGHL on the humerus and scapula were marked arthroscopically with copper wires to aid in identification of the AB-IGHL geometry in the volumetric CT data. An approximate zero-load configuration for the AB-IGHL was then determined via palpation. This position corresponded to 60° abduction and 40° external rotation. The bones were fixed in this position and then transported for volumetric CT data acquisition. A volumetric CT image data set was acquired with the scan axis oriented along the superior-inferior axis of the scapula (slice thickness, 1 mm; field of view, 255 mm;
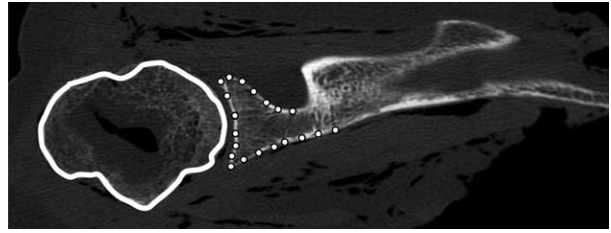

Figure 2 CT slice showing spline contour used to define the outer surface of the humerus and the individually digitized points on the scapula used to define the spline contour.

acquisition matrix, 512 × 512). The outer boundaries of the humerus, scapula, insertion site markers of the AB-IGHL, and registration blocks were hand-digitized on each CT slice, producing spline contours (Figure 2). Polygonal surface definitions were then constructed by stacking the individual contours and placing them together by use of Delaunay triangulation. The surfaces were then imported into a finite-element preprocessor (TrueGrid; XYZ Scientific, Livermore, CA). The polygonal surfaces of the bones were converted directly to rigid bodies for specification of shoulder kinematics. A hexahedral finite-element mesh was created for the AB-IGHL by use of contours of the reconstructed insertion sites and photographs of the AB-IGHL to determine geometry between insertion sites. The surfaces of the registration blocks were also reconstructed, and the identical local coordination systems were defined on the scapula and humerus. The computational time of the model was reduced by representing the scapula and humerus as separate collections of rigid shell elements, defining 2 rigid bodies for specification of experimentally measured kinematics.

Boundary conditions

The experimentally measured 3-dimensional kinematics of the registration blocks were used to prescribe the motion of the bones in the finite-element model. The coordinates of the Plexiglas registration blocks in the CT-defined coordinate system allowed correlation of kinematic measurements with geometric data.[5] The entire finite-element model was translated and rotated so that the global coordinate system was aligned with the coordinate system of the scapular registration block. Rigid body motion was specified in terms of incremental translations and rotations referenced to the coordinate systems of the registration blocks.[12,13] Incremental rotations were extracted from the transformation matrix by a combination of methods.[12,30] The finite-element mesh of the AB-IGHL was attached to the scapula and humerus by specifying rigid node sets at the proximal and distal ends of the finite-element mesh to be part of the same rigid body as the corresponding bone. This method essen-
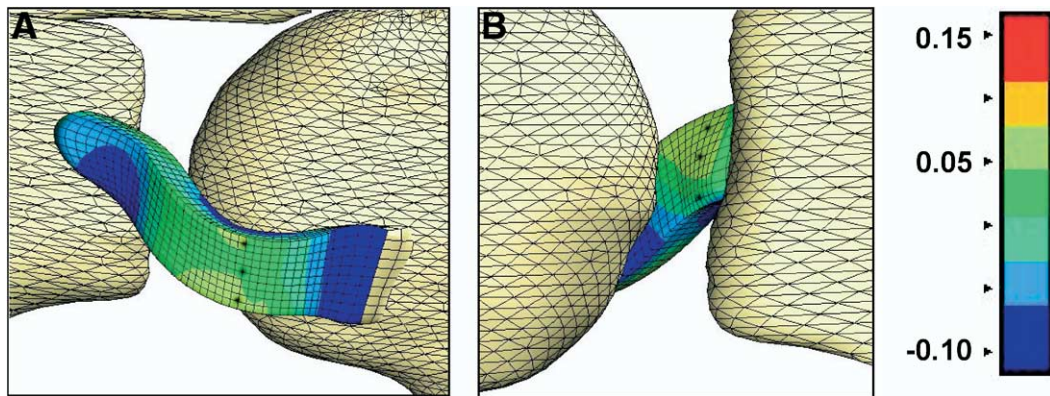
Figure 3 Fiber strain in the AB-IGHL at the initial kinematic position of the humerus with respect to the scapula. **A**, Anterior view of the glenohumeral joint with 3 locations marked for fiber strain measurements on the bursal side of the ligament. **B**, Posterior view of the glenohumeral joint with 3 locations marked for fiber strain measurements on the articular side of the ligament.

tially prescribed that the ends of the AB-IGHL must move with the humerus and scapula.

Contact and load transfer between the AB-IGHL and articular surface of the humeral head were modeled by use of the penalty method.[39] The magnitude of the in situ strain in the AB-IGHL was assumed to be zero at the configuration for the CT scan. The AB-IGHL was represented as transversely isotropic hyperelastic. This constitutive model has been used previously for several ligaments such as the medial collateral ligament and anterior cruciate ligament[37,38] and is appropriate for soft tissues with aligned collagen fibers. The AB-IGHL material is represented as a fiber-reinforced composite with this model. Fiber direction was assumed to run continuously between the insertion site locations on the humerus and scapula. Material coefficients for the constitutive model were obtained from experimental test data on a separate set of 10 shoulders.[20] The regions of the AB-IGHL near the insertion sites were modeled by use of the same material coefficients because material properties that are specific for the insertion sites were not available.

Finite-element analysis

The implicitly integrated finite-element code NIKE3D was used for all analyses.[13] The finite-element analysis was performed in 2 phases. During the first phase, the humerus was moved from the CT scanning position to the initial joint position at 60° of abduction, corresponding to the start of the experiment. During the second phase, the experimental shoulder kinematics corresponding to the simulated simple translation test were applied. An automatic time-stepping strategy was used, with iterations based on a quasi-Newton method[15] and convergence based on the L_2 displacement norm.[13,15] The post-

processing software GRIZ (Lawrence Livermore National Laboratory, Livermore, CA) was used to visualize the results. Finite-element predictions for strain along the local fiber direction (fiber strain) and von Mises stress were obtained throughout the entire AB-IGHL. The finite-element model was also used to predict the resultant force due to contact as the AB-IGHL wrapped around the humeral head.

RESULTS

Predicted fiber strains in the AB-IGHL were relatively small at the initial joint position of the simulated simple translation test. In addition, the strain was distributed nonuniformly in the ligament, with the highest fiber strain occurring near the insertion site on the scapula. On the basis of the strain distribution at the initial joint position, strain values were obtained from 2 locations along the length and 3 points across the width of the AB-IGHL. The first location was on the humeral side of the AB-IGHL, where the contact was initiated with the articular cartilage (bursal side of the tissue) (Figure 3, *A*). The second location was on the glenoid side of the AB-IGHL approximately 1 cm from the insertion site (articular side of the tissue) (Figure 3, *B*). These locations were chosen because they represented the regions of highest stress at this joint position. For the 6 locations examined at the initial position of 60° of abduction, neutral rotation, and neutral horizontal adduction, the predicted fiber strains were approximately 3% along the inferior edge on the humeral side and 4% on the glenoid side. Compressive strain occurred at locations where the AB-IGHL wrapped around the articular surface of the humeral head.

The fiber strain increased rapidly as the anterior load was applied to the humeral head and the AB-
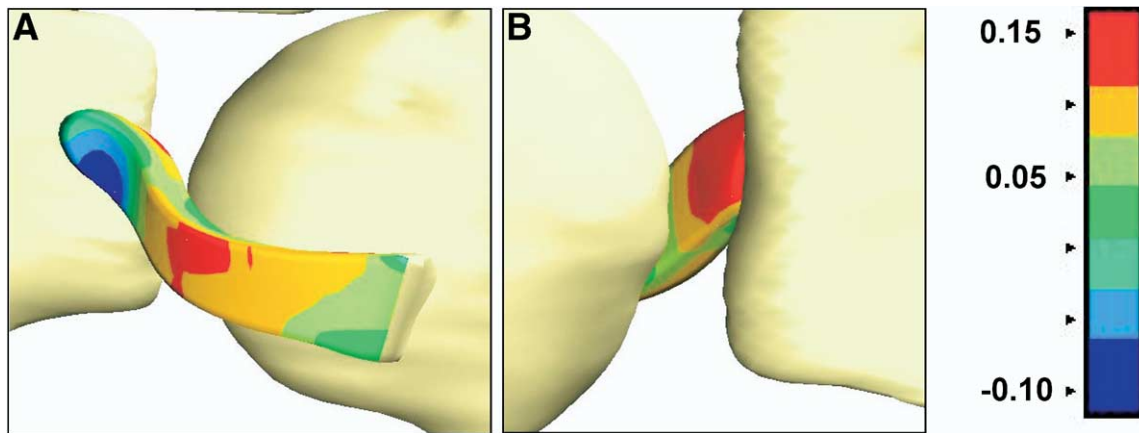
Figure 4 Fiber strain in the AB-IGHL at the maximum anterior translation of the humerus with respect to the scapula. **A**, Anterior view of the glenohumeral joint. **B**, Posterior view of the glenohumeral joint.
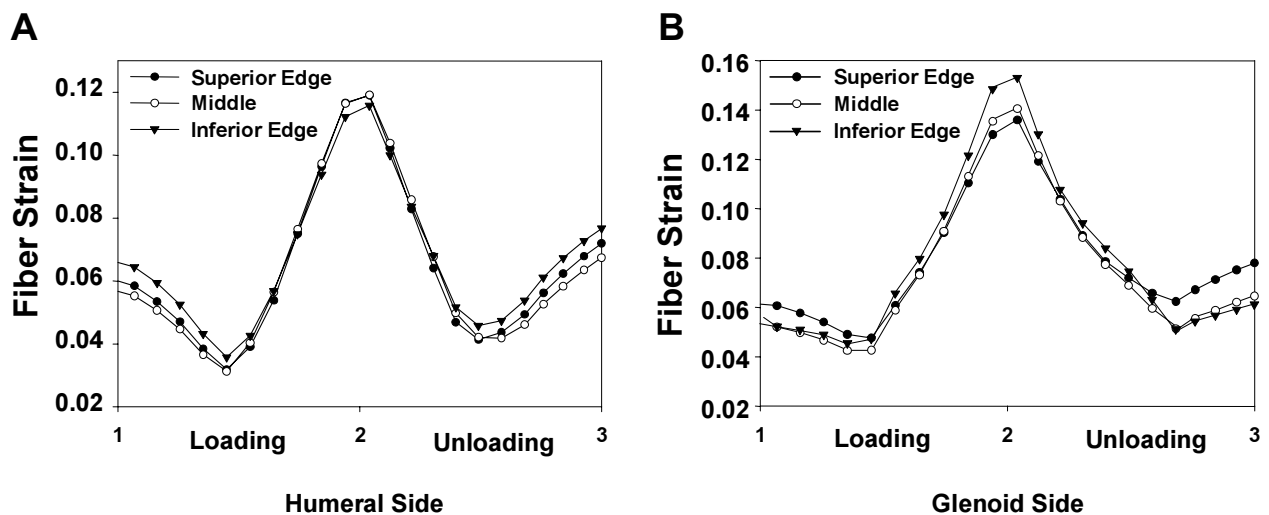

Figure 5 Fiber strain in the AB-IGHL as a function of applied kinematics for 3 measurement locations on the humeral side (**A**) and 3 measurement locations on the glenoid side (**B**).

IGHL deformed (Figures 4 and 5). These values increased uniformly at the 3 locations across the width of the ligament on the humeral and glenoid sides of the ligament. Fiber strains reached values of 12% along the inferior edge on the humeral side and 15% on the glenoid side at the maximum anterior translation of the humerus. During the unloading phase of the analysis, the fiber strains did not return to the same values at the beginning of the loading phase because the clinician did not return the joint to the exact same position at the end of the test. However, the fiber strain was within 1% to 2% for all measurement locations.

The von Mises stress in the AB-IGHL also increased rapidly as the humerus was translated anteriorly as a result of application of an anterior load (Figure 6).

The predicted values increased in a similar manner at the 3 locations on the humeral side and reached maximum values between 3.9 and 4.3 MPa. These sites were located where the AB-IGHL made contact with the articular surface of the humeral head. The maximum stress predicted for the locations on the glenoid side reached values of 4.1, 5.2, and 6.4 MPa at the inferior edge, superior location, and middle location, respectively. Once again, during the unloading phase, the von Mises stress at each location did not return to the values at the initiation of the loading phase but were within 1 MPa.

As the humerus was translated anteriorly, the AB-IGHL wrapped around the humerus and transferred load to the bone via contact. Contact force increased as the amount of anterior translation increased. Total
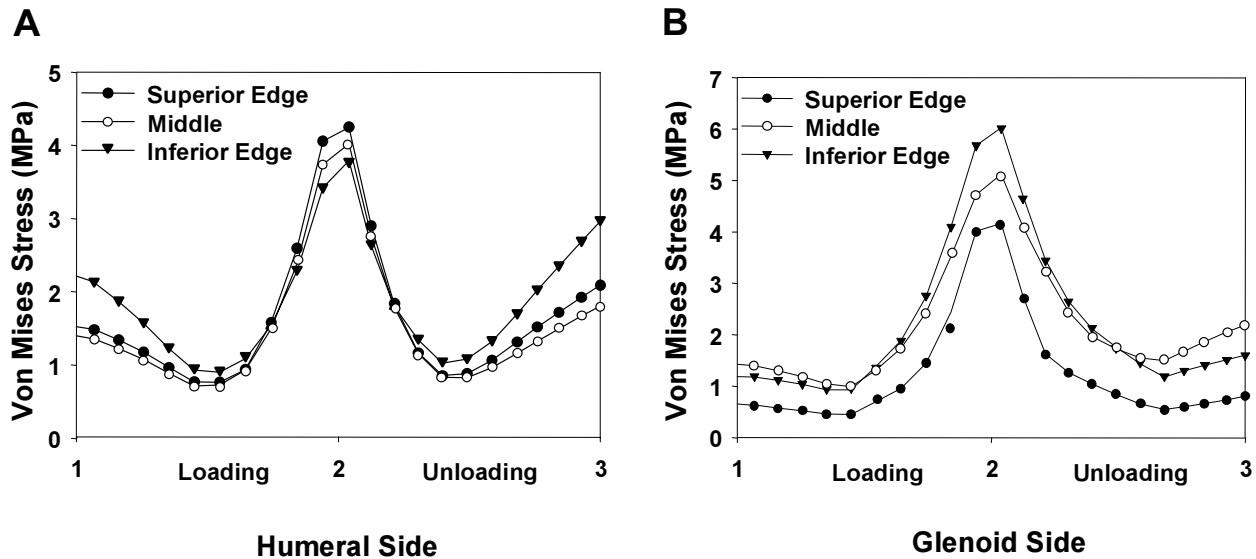
Figure 6 von Mises stress in the AB-IGHL as a function of applied kinematics for 3 measurement locations on the humeral side (**A**) and 3 measurement locations on the glenoid side (**B**).

contact force between the humerus and the ligament reached values of approximately 70 N at maximum anterior translation.

DISCUSSION

A finite-element model of the glenohumeral joint and AB-IGHL was developed, and the stress and strain in the AB-IGHL were predicted during application of an anterior load to the humerus. The computational approach used specimen-specific geometry and kinematics with average material properties and ligament geometry. The complex stress and strain distribution throughout the AB-IGHL supports our hypothesis. In addition, a significant amount of load was transferred from the AB-IGHL to the humerus as it wrapped around the articular surface of the humeral head.

The inferior edge of the AB-IGHL was subjected to high strains during anterior translation, primarily as a result of contact with the articular surface of the humeral head. The articular side of the AB-IGHL on the glenoid side also experienced large fiber strain, with the motion of the humerus tending to peel the ligament away from its scapular insertion. These 2 sites have been shown to comprise the greater percentage (82%) of the failure sites during tensile testing of the AB-IGHL, and the insertion site on the scapula is a common site for Bankart lesions.[18] These large strains at the insertion sites could have been caused by the direct attachment of the AB-IGHL to the bone by use of rigid nodes. However, our measurement locations were not directly adjacent to this stress concentration, minimizing its effect on the measurement sites.

In addition, the precise anatomy of the glenoid insertion site of the AB-IGHL is quite complex, with either a direct insertion to the labrum and some fibers extending along the glenoid neck or solely from the glenoid neck.[17] The properties at the insertion sites were not included in our study because these properties are unknown. However, the high fiber strains near the scapular insertion sites correlate well with previous studies[17,18] and suggest that future models should create a detailed structural model of the insertion sites to examine failure mechanisms resulting in Bankart lesions and repair procedures.

The magnitude of the predicted strains and stresses during the simulated simple translation test are within the range of data from previous experimental studies that measured strain during tensile tests or functional loading experiments. Several studies have examined the structural properties of the bone–AB-IGHL–bone complex or the mechanical properties of the midsubstance of the AB-IGHL. The elongation of the complex was approximately 25%,[1,18] and the strain and stress in the midsubstance of the AB-IGHL ranged from 7.2% to 10.9% and 5.5 to 8.5 MPa, respectively.[1,18,31] In our study, predicted values of maximum fiber strain reached 12% to 15% and maximum stresses reached 4.3 to 6.4 MPa. The computational results are within the functional regions of the load elongation and stress-strain curves determined by the previous studies, especially given that our maximum strain values occurred closer to the insertion sites rather than the midsubstance of the AB-IGHL. Experimental studies have also demonstrated that larger strains are found near the insertion sites compared with the midsubstance.[1,40] These comparisons demonstrate

that the computational approach provided reasonable predictions of strain in the AB-IGHL.

The strain in the AB-IGHL has also been estimated by use of Hall-effect strain transducers,[24] mercury strain gages,[2] and stereoradiogrammetry[14] during application of loads to the glenohumeral joint in previous studies. These studies suggest that the strain in the AB-IGHL is approximately 9% during external rotation of the humerus at 90° of abduction[24] and could reach values over 30% during a simulated apprehension examination.[2] However, peak strains near the glenoid and humeral insertion sites reached values of 31% and 28%, respectively, at 60° of abduction and 18 mm of anterior subluxation. Differences between the results of our study and the previous experimental results can be attributed to the loading conditions, strain measurement technique, and amount of capsule present. However, our data similarly suggest that the strain distribution varies throughout the AB-IGHL and the location of strain measurement is an important parameter.

This study is limited by the fact that only a portion of the shoulder capsule was modeled. Therefore, the load sharing between the AB-IGHL and the remainder of the capsule was not represented. This could influence the stress, strain, and load transfer mechanisms at each joint position. Furthermore, only 1 set of geometry was used in the computational analyses. Additional specimens should be examined with this methodology, and more specimen-specific parameters should be included, such as a larger portion of the glenohumeral capsule and the actual geometry for the reference configuration of the capsule (zero-strain state). Finally, the predictions from the finite-element model should be validated by use of experimental data instead of only comparing results with the strain data in the literature.

Problems encountered during finite-element analysis included excessive bending and buckling of the mesh as experimental kinematics were applied because the AB-IGHL is not always loaded. The hexahedral elements that composed the finite-element mesh of the AB-IGHL tended to "invert" during the nonlinear solution procedure, which led to numerical problems with convergence of the finite-element code. One possible solution to this problem is the use of shell elements.[9,27] Because shell elements are essentially 2-dimensional (although the thickness is taken into account for stress and strain calculations), element inversion resulting from the application of large bending strains is rarely a problem. They also have the added benefit of enhanced flexibility in bending in comparison to hexahedral elements and thus provide a better representation of the physics of thin structures such as the glenohumeral capsule. Shell elements are recommended for future computational analyses of the glenohumeral capsule.

The computational analyses performed in this study represent the first effort to model a portion of the glenohumeral capsule as a continuous 3-dimensional structure by use of finite-element analyses. This approach will serve as a first critical step toward development of a subject-specific model of the entire glenohumeral capsule. These types of models could lead to new biomechanically based strategies to improve diagnostic and surgical repair protocols for the glenohumeral capsule after shoulder dislocation. In the long term, our models could also be applied to study the healing process after injury and surgical repair.

REFERENCES

1. Bigliani LU, Pollock RG, Soslowsky LJ, et al. Tensile properties of the inferior glenohumeral ligament. J Orthop Res 1992;10:187-97.
2. Brenneke SL, Reid J, Ching RP, Wheeler DL. Glenohumeral kinematics and capsulo-ligamentous strain resulting from laxity exams. Clin Biomech (Bristol, Avon) 2000;15:735-42.
3. Debski RE, Wong EK, Woo SL-Y, et al. In situ force distribution in the glenohumeral joint capsule during anterior-posterior loading. J Orthop Res 1999;17:769-76.
4. Ferrari DA. Capsular ligaments of the shoulder. Anatomical and functional study of the anterior superior capsule. Am J Sports Med 1990;18:20-4.
5. Fischer KJ, Manson TT, Pfaeffle HJ, Tomaino MM, Woo SL. A method for measuring joint kinematics designed for accurate registration of kinematic data to models constructed from CT data. J Biomech 2001;34:377-83.
6. Harryman DT II, Sidles JA, Harris SL, Matsen FA III. The role of the rotator interval capsule in passive motion and stability of the shoulder. J Bone Joint Surg Am 1992;74:53-66.
7. Hoffmeyer P, Browne A, Korinek S, Morrey BF, An KN. Stabilizing mechanism of the glenohumeral ligaments. Biomed Sci Instrum 1990;26:49-52.
8. Howell SM, Galinat BJ, Renzi AJ, Marone PJ. Normal and abnormal mechanics of the glenohumeral joint in the horizontal plane. J Bone Joint Surg Am 1988;70:227-32.
9. Hughes TJR, Liu WK. Nonlinear finite element analysis of shells: part I. Three-dimensional shells. Comp Meth Appl Mech Eng 1981;26:331-62.
10. Inman VT, Saunders JB, Abbott LC. Observations on the function of the shoulder joint. J Bone Joint Surg Am 1944;26:1-30.
11. Lee TQ, Black AD, Tibone JE, McMahon PJ. Release of the coracoacromial ligament can lead to glenohumeral laxity: a biomechanical study. J Shoulder Elbow Surg 2001;10:68-72.
12. Maker BN. UCRL-JC-1198621-8. Rigid bodies for metal forming analysis with NIKE3D. Livermore (CA): University of California, Lawrence Livermore National Laboratory; 1995. p. 1-8.
13. Maker BN, Ferencz RM, Hallquist JO, editors. NIKE3D: a nonlinear, implicit, three-dimensional finite element code for solid and structural mechanics. Livermore (CA): Lawrence Livermore National Laboratory; 1990.
14. Malicky DM, Soslowsky LJ, Kuhn JE, et al. Total strain fields of the antero-inferior shoulder capsule under subluxation: a stereoradiogrammetric study. J Biomech Eng 2001;123:425-31.
15. Matthies H, Strang G. The solution of nonlinear finite element equations. Int J Numer Methods Engin 1979;14:1613-26.
16. McMahon PJ, Debski RE, Thompson WO, et al. Shoulder muscle forces and tendon excursions during glenohumeral abduction in the scapular plane. J Shoulder Elbow Surg 1995;4:199-208.
17. McMahon PJ, Ohland KH, Tibone J, Lee TQ. Variation in the histologic anatomy of the glenoid origin of the anterior band of the IGHL. Presented at the 45th Annual Meeting of the Orthopaedic

Research Society, February 1-4, 1999, Anaheim, CA. Transcripts of the Orthopaedic Research Society 1999;24:381.

18. McMahon PJ, Tibone JE, Cawley PW, et al. The anterior band of the inferior glenohumeral ligament: biomechanical properties from tensile testing in the position of apprehension. J Shoulder Elbow Surg 1998;7:467-71.

19. Miller MC, Smolinski PJ, Bains PK, Klein AH, Fu FH. A mathematical and experimental model of length change in the inferior glenohumeral ligament in the late cocking phase of pitching. Presented at the 37th Annual Meeting of the Orthopaedic Research Society, March 4-7, 1991, Anaheim, CA. Transcripts of the Orthopaedic Research Society 1991;16:609.

20. Moore SM, McMahon PJ, Debski RE. Bi-directional mechanical properties of the axillary pouch of the glenohumeral capsule: implications for modeling and surgical repair. J Biomech Eng 2004;126:284-8.

21. Moseley H, Overgaard B. The anterior capsular mechanism in recurrent anterior dislocation of the shoulder: morphological and clinical studies with special reference to the glenoid labrum and glenohumeral ligaments. J Bone Joint Surg Br 1962;44:913-27.

22. O'Brien SJ, Arnoczsky SP, Warren RF, Rozbruch SR. Developmental anatomy of the shoulder and anatomy of the glenohumeral joint. In: Rockwood CA, editor. The shoulder. Philadelphia: Saunders; 1990. p. 1-33.

23. O'Brien SJ, Neves MC, Arnoczky SP, et al. The anatomy and histology of the inferior glenohumeral ligament complex of the shoulder. Am J Sports Med 1990;18:449-56.

24. O'Connell PW, Nuber GW, Mileski RA, Lautenschlager E. The contribution of the glenohumeral ligaments to anterior stability of the shoulder joint. Am J Sports Med 1990;18:579-84.

25. Peat M. Functional anatomy of the shoulder complex. Phys Ther 1986;66:1855-65.

26. Poppen NK, Walker PS. Normal and abnormal motion of the shoulder. J Bone Joint Surg Am 1976;58:195-201.

27. Puso MA, Weiss JA, Maker BN, Schauer DA. A transversely isotropic hyperelastic shell finite element. Presented at the American Society of Mechanical Engineers, June 28-July 2, 1995, Beaver Creek, CO. ASME Bioengineering Conference 1995; 29:103-4.

28. Reis MT, Tibone JE, McMahon PJ, Lee TQ. Cadaveric study of glenohumeral translation using electromagnetic sensors. Clin Orthop 2002;400:88-92.

29. Rockwood CA, Matsen FA III, Wirth MA, Harryman DT II, editors. The shoulder. Philadelphia: Saunders; 1998.

30. Simo JC, Vu-Quoc L. On the dynamics in space of rods undergoing large motions: a geometrically exact approach. Comp Meth Appl Mech Eng 1988;66:125-61.

31. Stefko JM, Tibone JE, Cawley PW, ElAttrache NE, McMahon PJ. Strain of the anterior band of the inferior glenohumeral ligament during capsule failure. J Shoulder Elbow Surg 1997;6:473-9.

32. Terry GC, Hammon D, France P, Norwood LA. The stabilizing function of passive shoulder restraints. Am J Sports Med 1991; 19:26-34.

33. Tibone JE, Lee TQ, Black AD, Sandusky MD, McMahon PJ. Glenohumeral translation after arthroscopic thermal capsuloplasty with a radiofrequency probe. J Shoulder Elbow Surg 2000; 9:514-8.

34. Tibone JE, Lee TQ, Csintalan RP, Dettling J, McMahon PJ. Quantitative assessment of glenohumeral translation. Clin Orthop 2002;400:93-7.

35. Turkel SJ, Panio MW, Marshall JL, Girgis FG. Stabilizing mechanisms preventing anterior dislocation of the glenohumeral joint. J Bone Joint Surg Am 1981;63:1208-17.

36. Warner JJP, Caborn DN, Berger R, Fu FH, Seel M. Dynamic capsuloligamentous anatomy of the glenohumeral joint. J Shoulder Elbow Surg 1993;2:115-33.

37. Weiss JA, Gardiner JC. Computational modeling of ligament mechanics. Crit Rev Biomed Eng 2001;29:303-71.

38. Weiss JA, Maker BN, Govindjee S. Finite element implementation of incompressible, transversely isotropic hyperelasticity. Comp Meth Appl Mech Eng 1996;135:107-28.

39. Weiss JA, Schauer DA, Gardiner JC. Modeling contact in biological joints using penalty and augmented Lagrangian methods. Presented at the American Society of Mechanical Engineers, November 1996, Atlanta, GA. ASME Winter Annual Meeting 1996;347-8.

40. Woo SL-Y, Maynard J, Butler D, et al. Ligament, tendon, and joint capsule insertions to bone. In: Buckwalter JA, editor. Injury and repair of the musculoskeletal soft tissues. Park Ridge (IL): American Academy of Orthopaedic Surgeons; 1987. p. 133-66.

41. Zeminski J. Development of a combined analytical and experimental approach to reproduce knee kinematics for the evaluation of anterior cruciate ligament function. In: Mechanical engineering. Pittsburgh: University of Pittsburgh; 2001. pp. 52-6.